

PAPER • OPEN ACCESS

Microscopic nature of crystal phase quantum dots in ultrathin GaAs nanowires by nanoscale luminescence characterization

To cite this article: Bernhard Loitsch *et al* 2016 *New J. Phys.* **18** 063009

View the [article online](#) for updates and enhancements.

Related content

- [Efficient methodology to correlate structural with optical properties of GaAs nanowires based on scanning electron microscopy](#)
Wan-Hsien Lin, Uwe Jahn, Hanno Küpers *et al.*
- [Effect of V/III ratio on the structural and optical properties of self-catalysed GaAs nanowires](#)
L Ahtapodov, A M Munshi, J S Nilsen *et al.*
- [A review on III–V core–multishell nanowires: growth, properties, and applications](#)
Miquel Royo, Marta De Luca, Riccardo Rurali *et al.*

Recent citations

- [Efficient methodology to correlate structural with optical properties of GaAs nanowires based on scanning electron microscopy](#)
Wan-Hsien Lin *et al*
- [The effect of magnetic field on free and bound exciton luminescence in GaAs/AlGaAs multiple quantum well structures: a quantitative study on the estimation of ultra-low disorder](#)
S Haldar *et al*



PAPER

Microscopic nature of crystal phase quantum dots in ultrathin GaAs nanowires by nanoscale luminescence characterization

OPEN ACCESS

RECEIVED
2 March 2016REVISED
22 April 2016ACCEPTED FOR PUBLICATION
20 May 2016PUBLISHED
9 June 2016

Original content from this work may be used under the terms of the [Creative Commons Attribution 3.0 licence](#).

Any further distribution of this work must maintain attribution to the author(s) and the title of the work, journal citation and DOI.

Bernhard Loitsch¹, Marcus Müller², Julia Winner¹, Peter Veit², Daniel Rudolph¹, Gerhard Abstreiter¹, Jonathan J Finley¹, Frank Bertram², Jürgen Christen² and Gregor Koblmüller¹¹ Walter Schottky Institute, Physik Department, and Nanosystems Initiative Munich, Technische Universität München, Am Coulombwall 4, D-85748 Garching, Germany² Institute of Experimental Physics, Otto-von-Guericke-University Magdeburg, Universitätsplatz 2, D-39106 Magdeburg, GermanyE-mail: bernhard.loitsch@wsi.tum.de and marcus.mueller@ovgu.de**Keywords:** GaAs, nanowires, crystal phase polytypism, cathodoluminescence, photoluminescence, quantum dotsSupplementary material for this article is available [online](#)**Abstract**

Crystal phase quantum dots (CPQD) embedded in a nanowire (NW) geometry have recently emerged as efficient single photon emitters. In typical III–V semiconductor NWs such CPQDs are linked to the well-known zincblende (ZB)/wurtzite (WZ) polytypism that occurs mostly randomly along the NW axis, making it difficult to assess the exact position and microscopic nature of a particular emitter. Here, we employ highly spatially-resolved cathodoluminescence (CL) spectroscopy directly in a scanning transmission electron microscope to unambiguously identify type, microscopic nature, position and luminescence characteristics of single polytype defects in ultrathin GaAs–AlGaAs core–shell NWs with nanometer-scale resolution. Importantly, we find that individual twin defects (1 ML-inclusion of WZ in a ZB crystal) are the predominant source for QD emission, where the spectral position depends sensitively on the strength of radial confinement by the ultrathin GaAs NW core. By analyzing the temperature-dependent luminescence properties of a ~ 1 ML thick/7 nm wide twin-defect CPQD, we determine a thermal activation energy of ~ 7.4 meV for the confined excitons, as well as an evolution in linewidth that reflects phonon-mediated broadening processes, corroborating the QD-like behavior. Our findings also reveal the presence of effective carrier diffusion in-between isolated CPQDs.

Introduction

Freestanding III–V semiconductor nanowires (NW) are well known for their strong propensity for polytypism characterized by the coexistence of different crystal phases along their growth axis [1, 2]. In particular, wurtzite (WZ) and zincblende (ZB) phases as well as their intermixed structures are readily observed in almost the entire family of III–V semiconductor NWs, including arsenide (e.g. GaAs, InAs) [2–6], phosphide (e.g. InP, GaP) [7–9], and antimonide-based (e.g. InSb) materials [10], when grown along the common $\langle 111 \rangle$ orientations. Such crystal phase polytypism exhibits significant impact on the properties of functional NW devices [6, 8, 11], and further opens important opportunities in designing novel crystal phase heterostructures by exploiting the different electronic band structures and band-offsets of the WZ and ZB phases [12, 13]. In a bulk-like configuration, the WZ–ZB interface is well known to exhibit a type-II band alignment, with the conduction and valence bands in WZ being higher than in the ZB phase [4, 12, 13]. Consequently, in the limit of short ZB inclusions in WZ-phase NWs (or vice versa WZ inclusions in ZB-phase NWs), this leads to confinement of charge carriers in the growth direction [4, 6, 14, 15]. Attractive applications that directly exploit the carrier confinement at WZ/ZB-interfaces are so-called crystal phase quantum dots (CPQD) as first illustrated for InP-based NWs [15]. QDs integrated in a NW geometry open a pathway towards efficient single photon sources, due to the highly enhanced light extraction efficiency as demonstrated e.g. for heterostructure-type QDs [16–18].

The realization of WZ/ZB-CPQDs with high-brightness and indistinguishable single photon emission has been also attempted in the important GaAs-based NW material system. However, in conventional GaAs NWs (typical diameters of >30 nm, that is, larger than the excitonic Bohr radius), the carriers are not sufficiently confined in the direction perpendicular to the NW axis. Also, the type-II band alignment at the WZ/ZB-interface induces only indirect excitonic transitions with very long lifetimes ($>$ several ns) due to the reduced overlap of electron and hole wave functions [4, 14, 19–22]. Only very recently, first evidence was provided for bright and spectrally sharp single photon emitters from CPQDs in GaAs NWs with excitons confined in all three dimensions and with temporal characteristics exhibiting very fast lifetimes [23]. This was achieved by fabricating ultrathin, ~ 10 nm wide GaAs–AlGaAs core–shell NWs with a random distribution of mixed WZ/ZB crystal phases, rotational twins and stacking defects [23, 24]. Although WZ/ZB-like crystal defects have been put forward as the most likely origin for the sharp emission characteristics [23], the exact type, nature and position of the corresponding luminescence center has remained elusive.

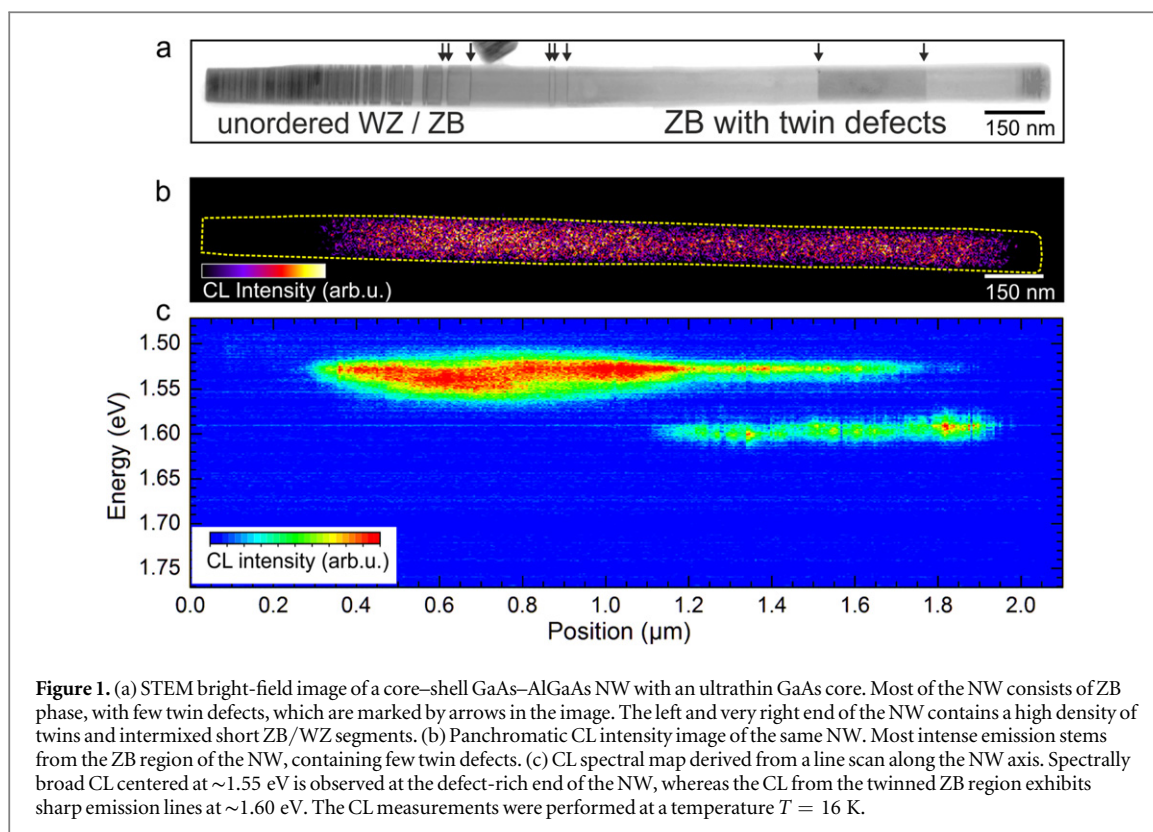
To exactly pin down these features is, however, complicated mainly by two effects: (a) crystal phase mixing of WZ/ZB phases occurs rather statistically along the NW axis, while deterministic control of type and position of crystal phase defect is still difficult in the common growth processes of GaAs NWs; (b) most of the standard techniques employed to directly correlate the microstructure of single NW with the optical properties are not of sufficiently high spatial resolution. Although there has been a significant body of work using correlated high-resolution transmission electron microscopy (TEM)/micro-photoluminescence (μ -PL) to identify the emission properties of different polytype inclusions and defects in GaAs NWs [4, 14, 22–24], the data represents mostly an average over relatively wide NW segments (typically >1 μ m, that is, resolution-limit of μ -PL). This makes it difficult to probe the exact nature and position of the respective luminescence center. Fortunately, ultrahigh-resolution analytical capabilities combining spatially-resolved cathodoluminescence (CL) spectroscopy directly with scanning-TEM (STEM) have very recently become available to exactly identify type, microscopic nature, position and luminescence characteristics of single crystal defects at the nanoscale with resolution in the few-nm range [25]. While, so far, these capabilities have been demonstrated almost exclusively in group-III nitride based quantum nanostructures emitting in the visible to ultraviolet spectral (vis–UV) range [25–28], only few attempts have been made to explore nanoscale materials and defects emitting in the infrared [29].

In this study, we demonstrate ultrahigh-spatially resolved STEM-CL on single GaAs–AlGaAs core–shell NWs with embedded CPQDs. By directly correlating the polytype defect structure with the spectrally sharp emitters localized along the length of the ultrathin GaAs NW core, we identify individual rotational twin defects as the dominant source for QD-like emission. In addition, by performing temperature-dependent luminescence experiments, we quantitatively determine the localization energies of the excitons in single twin defects and provide direct insights in the dynamics of charge carriers in the CPQDs inside strongly confined 1D-like NWs.

Methods

The investigated GaAs–AlGaAs core–shell NWs were fabricated by molecular beam epitaxy (MBE) on a Si (111) wafer. The Si wafer was covered with a ~ 2 nm thick SiO_2 layer containing nanometer sized pinholes in the SiO_2 layer, as induced by wet chemical etching in hydrofluoric acid, to define random nucleation sites for the NWs. In general, nucleation and growth of well controlled III–V NWs on Si substrate is quite challenging and the method demonstrated here is one of several different fabrication techniques [30–34]. In our MBE process, the GaAs NW cores were grown via the vapor–liquid–solid growth mode where Ga-droplets act as autocatalysts. For this growth step, a substrate temperature of 610 °C, a Ga-flux of 0.025 nm s^{-1} and an As-flux of 0.103 nm s^{-1} (beam equivalent pressure (BEP) of 1.90×10^{-6} mbar) was chosen. After 40 min of NW core growth, the Ga and As fluxes were turned off and the substrate temperature was increased to 680 °C for 30 min to thin down the NW diameter to ~ 10 nm via thermal evaporation [21]. Finally, to passivate surface states and thereby inducing strong luminescence efficiency in the NW [35], the NWs were overgrown with a 35 nm thick $\text{Al}_{0.25}\text{Ga}_{0.75}$. As shell followed by a 10 nm thick GaAs capping layer. For shell overgrowth the substrate temperature was decreased to 490 °C. The shell was grown at Ga and Al fluxes of 0.017 nm s^{-1} and 0.0057 nm s^{-1} , respectively, and the As flux was set to 1.90 nm s^{-1} (BEP 3.50×10^{-5} mbar), as adapted from optimized planar AlGaAs/GaAs growth on (110) GaAs [36].

To perform low-temperature ($T = 16$ K) STEM-CL characterization along the length of individual NWs the as grown NWs were mechanically transferred onto carbon-coated TEM grids and mounted on a modified liquid Helium TEM cryo-sample holder. Low-temperature CL was directly applied in a STEM FEI STEM Tecnai F20 to correlate the crystalline real structure of the core–shell NW with the luminescence properties with nanometer-scale resolution. In STEM mode, the focused electron beam is scanned over the NW while the emitted light is



collected by a parabolic aluminum mirror and focused onto the entrance slit of the grating monochromator MonoCL4 (Gatan) [26, 27]. The collected light is detected by a liquid N₂ cooled silicon charge-coupled device (CCD). This results in a three-dimensional data set $I_{CL}(x, \lambda)$ with a spectral resolution of 0.6 nm. Simultaneous to the detection of the CL-signal, a bright field and a high-angle annular dark field (HAADF) electron detector are used for acquiring the STEM image. The STEM acceleration voltage was set to 80 keV to prevent luminescence degradation. The electron excitation beam has a diameter of ~ 0.6 nm. Due to scattering of primary electrons in the sample we estimate that the effective excitation spot size is widened to a diameter of ~ 15 for a 80 nm thick GaAs film (Goldstein range) [37].

For temperature dependent μ -PL measurements NWs from the same sample were dispersed onto silicon substrate which was then mounted in a liquid He flow cryostat. The temperature can be controlled by the liquid helium flow and is monitored with a thermocouple. For optical excitation a 654 nm pulsed diode laser emitting 100 ps pulses with a repetition rate of 40 MHz is focused through an objective onto the sample, yielding a diffraction limited spot of ~ 1 μ m. The excitation laser was adjusted to a low power of 180 nW throughout the experiments presented here. The PL is collected confocally through the same objective and analyzed in a 0.5 m focal length monochromator (Princeton Instruments Acton, 1200 mm⁻¹ grating) equipped with a liquid N₂ cooled CCD detector.

Results and discussion

A representative bright-field STEM image of a single GaAs–AlGaAs core-shell NW is shown in figure 1(a). The contrast alternations directly indicate that there is a variation in crystal structure along the NW axis. In particular, the NW consists of predominantly ZB crystal structure with up to few hundred-nm long rotational twins which are separated by single twin defects (marked by arrows in figure 1), that is, the inclusion of a monolayer of WZ. Towards the left end of the NW as well as the very right end (< 100 nm wide region) the crystal structure becomes more disordered with a higher density of twin defects and also short WZ segments embedded in the ZB crystal, as verified in our earlier work by correlated selected area diffraction imaging [24, 38]. Furthermore, the GaAs NW core is characterized by slight tapering along the growth axis, as confirmed by more detailed STEM analysis (see supporting information). Essentially, from the left to the right end of the NW, the NW core diameter decreases from 14 ± 2 nm to 7 ± 2 nm, which is a consequence of the varying Ga droplet diameter during the self-catalyzed growth conditions used for the GaAs NW core growth [38].

A panchromatic CL intensity map of the same NW, as recorded at 16 K under an electron excitation current of 69 pA is further shown in figure 1(b). It can be clearly seen that the luminescence intensity reaches a maximum in the central part of the NW, which corresponds to regions where ZB crystal phase and individual twin defects prevail. In contrast, we obtain only weak CL intensity for excitation in the highly defective left and very right end of the NW where random crystal phase defects and intermixing with WZ phase are more prevalent. To visualize the optical properties of the WZ-segments and the twin defects on a nanoscale, a CL line scan was performed while the convergent electron beam was scanned axially along the NW. In figure 1(c) the color coded CL intensity is plotted as a function of axial position and emission wavelength. Clearly, the CL line scan yields different emission energy distributions between the right and left parts of the NW: while we observe discrete sharp lines at an energy of ~ 1.60 eV in the right part of the NW, excitation in the left part of the NW yields also CL that is spectrally centered at ~ 1.55 eV and which has a broad and continuous shape.

The spectral change along the NW can be directly associated with the changing crystal structure and core diameter which determine the electronic band-structure along the NW. The isolated twin defects in the predominant ZB-phase part of the NW represent effectively isolated CPQDs where the excitons are confined axially by the twin defect and radially by the ~ 7 – 10 nm core diameter, hence, leading to few discrete electronic states and distinct sharp QD-like transitions. The CL feature at ~ 1.55 eV is also present in this part of the NW, which we attribute to diffusion of the free carriers towards the left NW end, where the energetically lower transitions are predominant. This diffusion process is reasonable considering the relatively large carrier diffusion length in GaAs at low temperature (order of few hundred nm to $1 \mu\text{m}$) [39]. We elaborate more closely the effects of carrier diffusion in the NW via temperature-dependent PL measurements further below. In the region of higher twin defect density and WZ segments, e.g., towards the ~ 14 nm thick end of the NW, there is a higher density of transitions leading to an energetically broad luminescence from this part of the NW. Notably, we observe no sharp emission lines at the position of the twin defects located at $\sim 0.9 \mu\text{m}$. We attribute this observation to transfer of the charge carriers to the energetically lower transitions (1.55 eV) of the nearby defect-rich NW end. The continuous shape of the CL spectrum at around 1.55 eV differs from PL measurements of defect-rich NW segments in ultrathin GaAs NWs where one rather observes separated peaks in the spectrum, as will be presented below and has also been shown in a previous study [23]. This can be explained by the fact that the excitation density in CL is significantly larger than in μ -PL experiments and therefore the 0D states are filled up readily, such that their energetically discrete transitions are superimposed by recombination from the 1D-NW continuum. Furthermore, the CL from this region is at a comparatively lower energy at ~ 1.55 eV due to the weaker radial quantum confinement in the thick NW end.

To provide more detailed insights into the role of individual twin defects on the CL properties, we performed higher-resolution analysis around well-defined rotational twins under lower CL excitation density (19 pA electron excitation current). Figure 2(a) shows a corresponding STEM HAADF image recorded close to the right end of the NW. The micrograph reveals that this part of the NW consists of few hundred-nm long ZB segments, separated by two individual twin defects which are marked by arrows. Respective CL spectra recorded at different positions along this segment of the NW are presented in figure 2(b). The positions of the electron excitation spot are denoted as white rectangles in the STEM image of figure 2(a). The spectra consist of a few distinct sharp lines with linewidths down to below the resolution limit of the CL spectrometer (~ 4 meV). Most importantly, the positions of the most intense peaks, at 1.58 and 1.61 eV, directly correlate with the two marked twin defects in the NW. In particular, the intensity of the peak at 1.58 eV reaches maximum intensity for excitation close to the twin defect marked by the blue arrow, while the transition at 1.61 eV correlates with the twin defect marked by the red arrow. For the transition at 1.58 eV a slight shift in energy (barely above the resolution limit of the spectrometer) can be noted in the spectrum when comparing electron excitation directly on the twin defect (labeled as position number 5 in figure 2) with excitation in the vicinity of the twin defect. We attribute this shift to Coulomb interaction with excited electrons in the vicinity of the CPQD [23, 40]. These two observations, that is, the spatial coincidence of the twin defect with CL excitation position where the peak intensity reaches its maximum as well as the correlation of excitation position and shift in transition energy, clearly corroborate that the sharp QD-like transitions originate from single isolated twin defects. The fact that the sharp-line transitions do not only appear when the excitation spot is directly focused on the corresponding twin defect, but also for excitation in the proximity of the twin illustrates that the carrier diffusion length inside the ZB segment is at least half the segment length, i.e., > 150 nm, in agreement with previous reports [19, 39]. Interestingly, there is an energy difference of ~ 30 meV between the transitions associated to the two twin defects. We attribute this difference to a change in radial quantum confinement due to the variation of the NW core diameter along the investigated segment. Via STEM HAADF imaging we could determine the core diameter with an accuracy of ± 2 nm (see supporting information). For a ~ 7 nm thick NW core a change in radial confinement energy of ~ 30 meV corresponds to a change in core diameter of only 1.5 nm [24], which is within the accuracy of the STEM imaging. There is an additional emission feature present at ~ 1.59 eV which is denoted

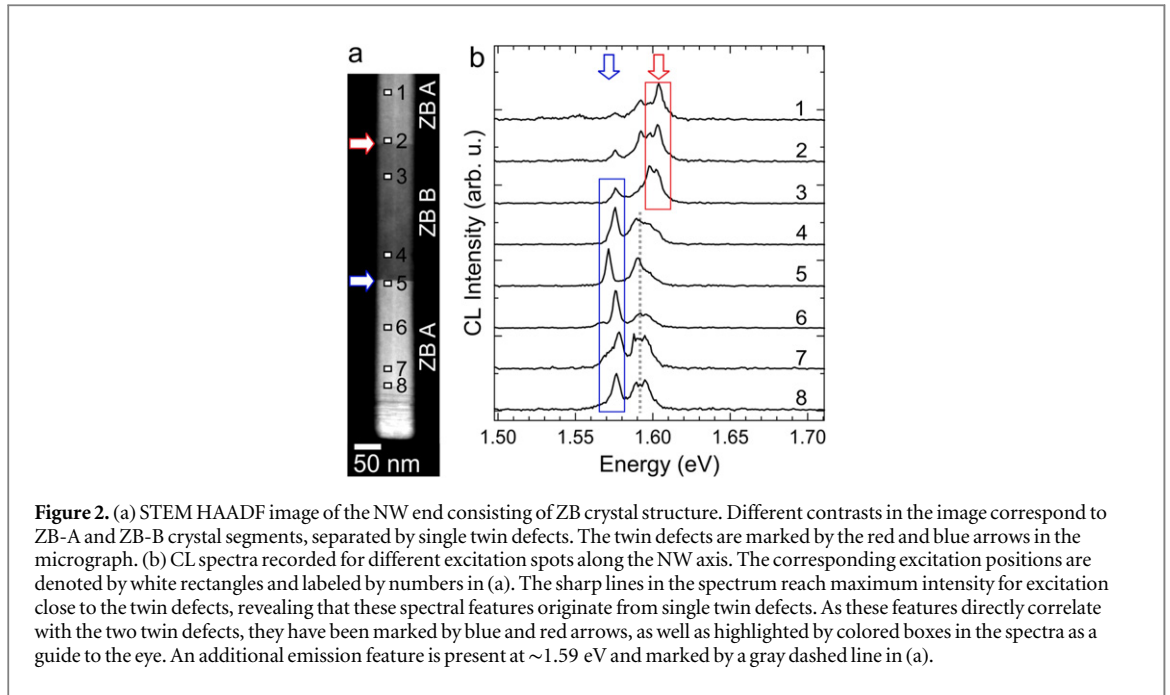


Figure 2. (a) STEM HAADF image of the NW end consisting of ZB crystal structure. Different contrasts in the image correspond to ZB-A and ZB-B crystal segments, separated by single twin defects. The twin defects are marked by the red and blue arrows in the micrograph. (b) CL spectra recorded for different excitation spots along the NW axis. The corresponding excitation positions are denoted by white rectangles and labeled by numbers in (a). The sharp lines in the spectrum reach maximum intensity for excitation close to the twin defects, revealing that these spectral features originate from single twin defects. As these features directly correlate with the two twin defects, they have been marked by blue and red arrows, as well as highlighted by colored boxes in the spectra as a guide to the eye. An additional emission feature is present at ~ 1.59 eV and marked by a gray dashed line in (a).

by the dashed line in figure 2. We speculate that this emission originates from crystal defects located at the very tip of the NW.

To further gain insights into the strength of the confinement potential of the individual twin defects, we examine in the following the carrier dynamics as a function of temperature. These experiments were performed using μ -PL spectroscopy which allows to vary the lattice temperature in the He flow cryostat. Here, we investigate PL spectra of a NW with very similar characteristics, as particularly shown in figure 3(a) for two distinct positions along the NW axis. Note that unlike in CL measurements, the spatial resolution in μ -PL is limited by the ~ 1 μm spot size of the excitation laser. Nevertheless, a clear difference can be observed between spectra recorded in the left and right parts of the NW plotted as red and blue curves, respectively. The PL from the right, thinner section of the NW (ZB-phase with few twin defects) consists of a dominant strongly blue-shifted sharp line at > 1.60 eV, similar to the observations by CL. On the other hand, the spectrum from the left, thicker and more defective section of the NW contains also multiple broader peaks at lower energies, which agrees well with the weaker confinement properties in this region as also found by the correlated CL-TEM data. As mentioned previously, the energetically lower lying transitions (~ 1.53 – 1.58 eV) appear much more as distinct peaks in the PL as compared to CL. We assign this difference to the comparatively low excitation power density of ~ 20 W cm^{-2} used in the PL experiments, where the localized states are not filled up as in the case of CL.

To study the temperature-dependent PL of the twin-defected region in more detail, we fix both excitation and detection to the right, thinner section of the NW. Due to the finite ~ 1 μm wide excitation spot size and carrier diffusion along the NW, the PL signal also contains the energetically lower transitions arising from the thick NW end (low-intensity features in the red curve of figure 3(a) as recorded at 10 K). The presence of both the twin-defect related sharp-line emission (at 1.635 eV) and the low-energy transitions are best represented in the logarithmic plot of figure 3(b), which depicts spectra recorded at temperatures ranging from 10 to 77 K. We note that the intensity of the sharp line emission at 1.635 eV quenches monotonically with increasing temperature, as expected for a QD-like emitter [41, 42]. In contrast, the intensity of the low-energy transitions does not decrease monotonically but reaches a maximum at elevated temperatures, as further discussed below. In addition, the low-energy transitions at ~ 1.55 eV do not continually red-shift in energy with increasing temperature, as indicated by the arrow symbols in figure 3(b). Instead, two of the transitions follow an ‘s-shape’ temperature dependence, that is, a red-shift followed by a blue-shift and final red-shift in transition energy, which is a characteristic behavior for highly defected GaAs NWs where the blue-shift is attributed to thermal activation of carriers to close-by narrow ZB/WZ-type quantum wells [20]. The absence of this anomalous behavior in the sharp-line emission center at ~ 1.63 eV, which exhibits rather a monotonic red-shift, supports our interpretation of an isolated twin defect QD.

For a more quantitative analysis of the variable PL intensity with temperature, the integrated intensities are plotted as a function of inverse temperature for the sharp-line transition at 1.635 eV (figure 4(a)), and the

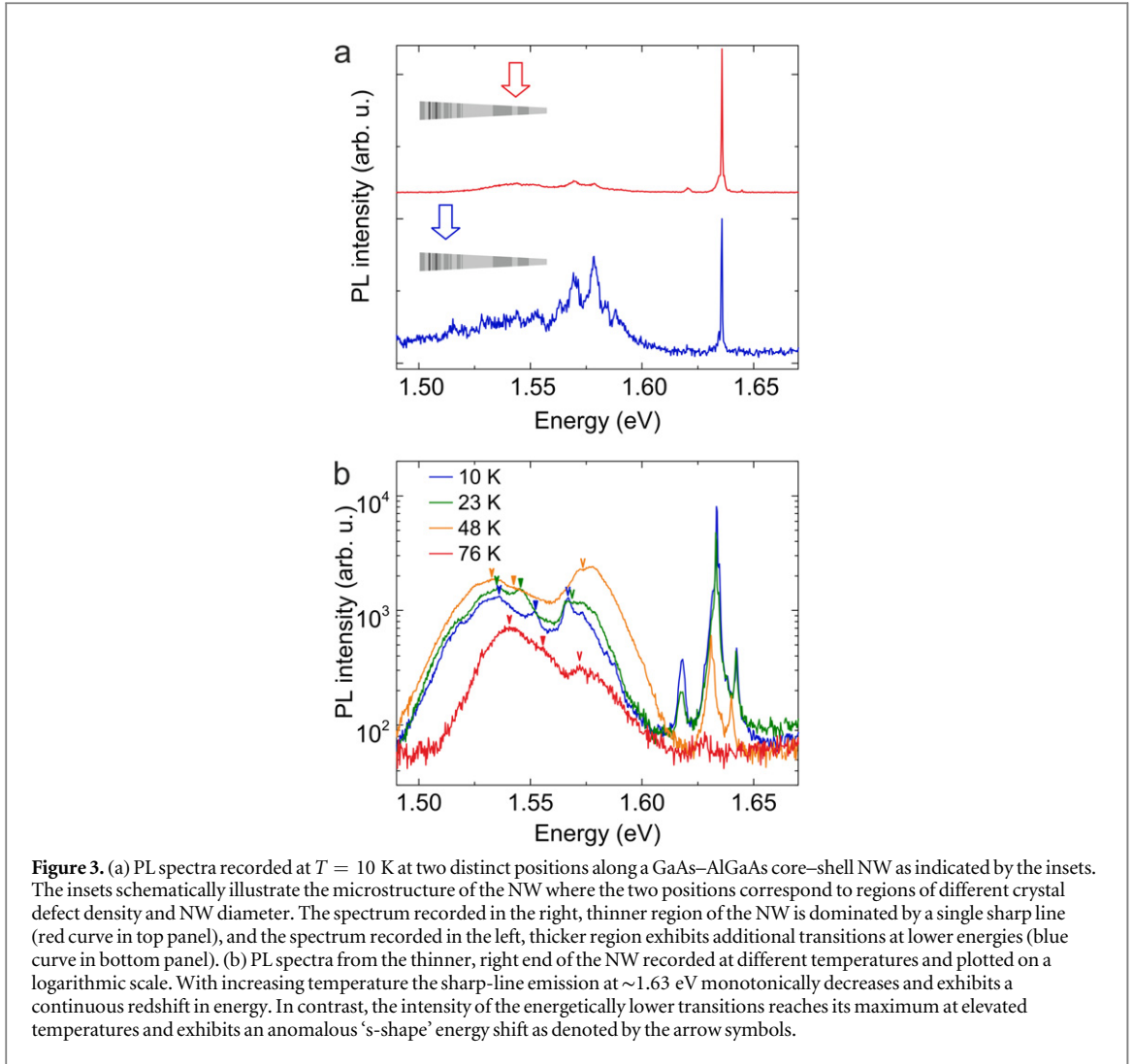


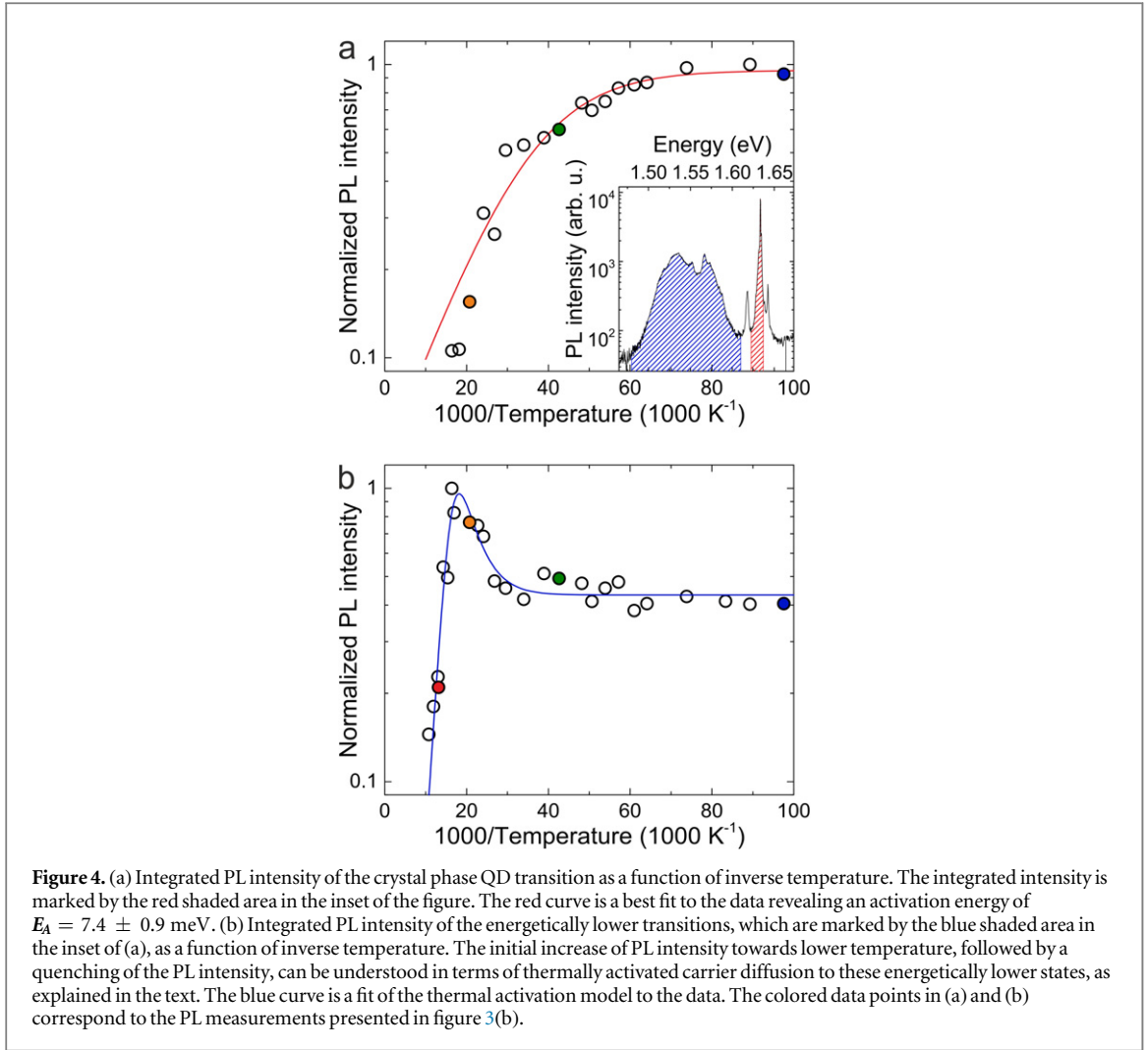
Figure 3. (a) PL spectra recorded at $T = 10$ K at two distinct positions along a GaAs–AlGaAs core–shell NW as indicated by the insets. The insets schematically illustrate the microstructure of the NW where the two positions correspond to regions of different crystal defect density and NW diameter. The spectrum recorded in the right, thinner region of the NW is dominated by a single sharp line (red curve in top panel), and the spectrum recorded in the left, thicker region exhibits additional transitions at lower energies (blue curve in bottom panel). (b) PL spectra from the thinner, right end of the NW recorded at different temperatures and plotted on a logarithmic scale. With increasing temperature the sharp-line emission at ~ 1.63 eV monotonically decreases and exhibits a continuous redshift in energy. In contrast, the intensity of the energetically lower transitions reaches its maximum at elevated temperatures and exhibits an anomalous ‘s-shape’ energy shift as denoted by the arrow symbols.

energetically lower transitions at ~ 1.55 eV (figure 4(b)). The integrated intensities were extracted for the respective peaks across the corresponding energy intervals given by the red and blue shaded area in the inset of figure 4(a). Clearly, the integrated intensity of the sharp-line transition at 1.635 eV quenches continually with increasing temperature. This behavior can be well described by a simple rate equation model, where we assume that the carriers localized in the twin-defect based CPQD become thermally activated to a non-radiative process via a Boltzmann temperature dependence (see supporting information) [43, 44]. As a result, the temperature-dependent quenching of the PL intensity can be described by the following relation

$$I(T) = \frac{I_0}{1 + C \cdot \exp\left(-\frac{E_A}{k_B T}\right)}.$$

Here E_A is the thermal activation energy and I_0 and C are fitting constants. The red curve in figure 4(a) is a best fit to the experimental data, from which we obtain an activation energy of $E_A = 7.4 \pm 0.9$ meV. This value is clearly above the binding energy $E_B = 4.2$ meV of free excitons in bulk GaAs [45], as expected due to the increased overlap of the electron and hole wave functions within the CPQD.

On the other hand, to describe the temperature-dependent PL intensity of the low-energy transitions from the defect-rich, left end of the NW, we include an additional contribution of charge carriers which are not directly optically excited into the radiative transition but are instead captured and thermally activated from an intermediate states in nearby CPQDs. The solution of the rate equation then leads to the following temperature dependent PL intensity



$$I(T) = \frac{I_0 + b \cdot \exp\left(-\frac{E_{A2}}{k_B T}\right)}{1 + C \cdot \exp\left(-\frac{E_{A1}}{k_B T}\right)}.$$

Again, C is a fitting constant and E_{A1} is the Boltzmann activation energy to a non-radiative recombination channel of the carriers. I_0 is a fitting constant which is proportional to the rate of carriers excited by the laser. The fitting constant b and the activation energy E_{A2} describe the thermal activation of carriers being fed into to the radiative process. Importantly, due to this additional contribution of carriers from localized states of nearby crystal defects, quenching occurs not monotonically but is superimposed by an initial increase of the PL intensity. From the fit to the experimental data, plotted by the blue curve in figure 4(b), we determine $E_{A1} = 62 \pm 6$ meV and $E_{A2} = 20 \pm 7$ meV. The activation energy E_{A1} is again significantly larger than the bulk GaAs exciton binding energy due to the localization in the crystal defects. Interestingly, it is also significantly larger than $E_A = 7.4 \pm 0.9$ meV of the sharp-line twin-defect based CPQD emitter from the thin NW region. This energy difference could be caused by a difference in the WZ/ZB band offset in the thicker NW region because of the modified radial confinement. In addition, there is also a high number of neighboring twin defects and WZ segments in the thicker NW region, where the thermally activated carriers may not only lead to a direct suppression of the PL intensity but also induce hopping into adjacent energetically higher defects from where they recombine radiatively. This interpretation is supported by the observed anomalous s-shape energy shift of these transitions, as discussed above. The onset of the increase in PL intensity (i.e., at $1000 T^{-1} \sim 30 K^{-1}$) as seen in figure 4(b) directly correlates with the onset of quenching of the energetically higher CPQDs (see figure 4(a)), which indicates the presence of carrier transfer from the twin defects to the thicker, more defective NW region. However, the activation energy E_{A2} is larger than the activation energy of the isolated twin-defect CPQDs. A possible explanation of this behavior is that both electrons and holes have to be thermally activated

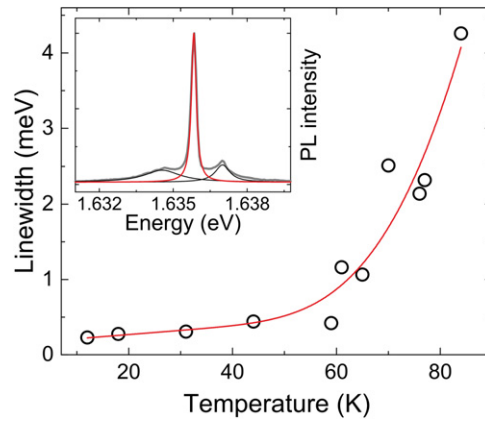


Figure 5. Evolution of the temperature dependence of the linewidth of the dominant CPQD transition at 1.635 eV. The linewidth was extracted from a fit of multiple Lorentzian curves to the PL spectrum, as shown in the inset. Black data points refer to experimental data, while the solid curve is a best fit to the data, revealing that the linewidth increases linearly with temperature at low temperature (acoustic phonon scattering) and super-linearly at high temperature (LO phonon scattering). The zero-phonon linewidth (extrapolation to 0 K) is found to be $\Gamma_0 = 152 \pm 35 \mu\text{eV}$.

from the QD and transferred to the thick NW region, unlike the situation of the quenching process of the QD, where the activation of only one carrier species is necessary. Another possible reason for the higher activation energy could also be energetic barriers, as in the form of other crystal defects, which have to be overcome by the carriers diffusing to the thicker NW region.

Finally, we present relevant temperature dependent dynamics of the twin-defect CPQDs by closely investigating the evolution of the linewidth of the sharp-line transition at 1.635 eV. By fitting multiple Lorentzian curves to the spectrum, as shown in the inset of figure 5(a), we extracted the full-width-at-half-maximum (FWHM) of the transition for different temperatures. The FWHM values increase with temperature which agrees favorably with the characteristic behavior of a QD: essentially, the behavior is described first by a linear increase at low temperatures due to acoustic phonon scattering followed by an exponential increase due to the generation of longitudinal-optical (LO) phonons [46–48]. For a quantitative analysis we fit the conventional function $\Gamma(T) = \Gamma_0 + \alpha \cdot T + b \cdot (\exp(E_{\text{LO}}/k_{\text{B}}T) - 1)^{-1}$ for thermal broadening of the QD linewidth. From the best fit to the data, which is plotted in figure 5(a), we determine the LO phonon energy $E_{\text{LO}} = 40 \pm 18 \text{ meV}$, which is in close agreement with the LO phonon energy of bulk GaAs of 36.25 meV [49]. We also determine an acoustic phonon scattering coefficient $\alpha = 6 \pm 1 \mu\text{eV K}^{-1}$ from the fit, which is in the range of typical values obtained for excitons in bulk GaAs and GaAs quantum wells [50]. The zero-phonon linewidth is found to be $\Gamma_0 = 152 \pm 35 \mu\text{eV}$, which lies above the natural linewidth corresponding to the previously determined CPQD lifetimes of few hundred ps [23]. This indicates that additional broadening mechanisms are present, such as coupling with nearby electronic states or scattering at charged impurities.

Conclusion

We unambiguously demonstrated that among the various WZ/ZB polytype combinations single twin defects formed inside ultrathin GaAs NWs are the dominant origin for CPQDs, as verified by high-resolution STEM cathodoluminescence. These findings are further corroborated by temperature-dependent luminescence studies of a well-defined, that is, ~ 1 ML thick/7 nm wide twin defect, which exhibits a thermal activation energy for the confined excitons nearly twice as large that for bulk GaAs as well as a temperature-dependent linewidth evolution directly reflecting phonon-mediated processes typical for a single semiconductor QD. In addition, the temperature-dependent studies further reveal that carrier diffusion along the ultrathin 1D-GaAs NW core leads to a carrier transfer between the QDs. These results provide important insights into the nature and confinement properties of novel CPQDs in III–V semiconductor NWs, which are considered as relevant candidates for future quantum information technologies.

Acknowledgments

The authors would like to thank B Mayer, J Wierzbowski, and M Kaniber for experimental support and helpful discussions. The work was supported financially by the Deutsche Forschungsgemeinschaft (SFB-631, SFB-787, and the Research Instrumentation Program INST 272/148-1), the Nanosystems Initiative Munich, the

TUM-IAS Focus group ‘Semiconductor Nanowires’, the International Graduate School for Science and Engineering (TUM-IGSSE), and the IBM International PhD Fellowship Program.

Supplementary data

This includes the measurement of the GaAs nanowire core diameter via high-angle annular dark-field scanning transmission electron microscopy and shows the energetic shift of the crystal phase quantum dot transition with temperature. Also the rate equation model for the temperature dependent photoluminescence is presented.

References

- [1] Glas F, Harmand J-C and Patriarche G 2007 Why does wurtzite form in nanowires of III-V zinc blende semiconductors? *Phys. Rev. Lett.* **99** 146101
- [2] Caroff P, Dick K A, Johansson J, Messing M E, Deppert K and Samuelson L 2009 Controlled polytypic and twin-plane superlattices in III-V nanowires *Nat. Nanotechnol.* **4** 50–5
- [3] Dubrovskii V G and Sibirev N V 2008 Growth thermodynamics of nanowires and its application to polytypism of zinc blende III-V nanowires *Phys. Rev. B* **77** 035414
- [4] Spirkoska D et al 2009 Structural and optical properties of high quality zinc-blende/wurtzite GaAs nanowire heterostructures *Phys. Rev. B* **80** 245325
- [5] Johansson J, Dick K A, Caroff P, Messing M E, Bolinsson J, Deppert K and Samuelson L 2010 Diameter dependence of the wurtzite–zinc blende transition in InAs nanowires *J. Phys. Chem. C* **114** 3837–42
- [6] Dayeh S A, Susac D, Kavanagh K L, Yu E T and Wang D 2009 Structural and room-temperature transport properties of zinc blende and wurtzite InAs nanowires *Adv. Funct. Mater.* **19** 2102–8
- [7] Algra R E, Verheijen M A, Borgström M T, Feiner L-F, Immink G, van Enckevort W J P, Vlieg E and Bakkers E P A M 2008 Twinning superlattices in indium phosphide nanowires *Nature* **456** 369–72
- [8] Joyce H J, Wong-Leung J, Gao Q, Tan H H and Jagadish C 2010 Phase perfection in zinc blende and wurtzite III-V nanowires using basic growth parameters *Nano Lett.* **10** 908–15
- [9] Assali S et al 2013 Direct band gap wurtzite gallium phosphide nanowires *Nano Lett.* **13** 1559–63
- [10] Kriegner D et al 2011 Unit cell structure of crystal polytypes in InAs and InSb nanowires *Nano Lett.* **11** 1483–9
- [11] Thelander C, Caroff P, Plissard S, Dey A W and Dick K A 2011 Effects of crystal phase mixing on the electrical properties of InAs nanowires *Nano Lett.* **11** 2424–9
- [12] Akiyama T, Yamashita T, Nakamura K and Ito T 2010 Band alignment tuning in twin-plane superlattices of semiconductor nanowires *Nano Lett.* **10** 4614–8
- [13] Belabbes A, Panse C, Furthmüller J and Bechstedt F 2012 Electronic bands of III-V semiconductor polytypes and their alignment *Phys. Rev. B* **86** 75208
- [14] Heiss M et al 2011 Direct correlation of crystal structure and optical properties in wurtzite/zinc-blende GaAs nanowire heterostructures *Phys. Rev. B* **83** 45303
- [15] Akopian N, Patriarche G, Liu L, Harmand J C and Zwiller V 2010 Crystal phase quantum dots *Nano Lett.* **10** 1198–201
- [16] Pelton M, Santori C, Vucković J, Zhang B, Solomon G S, Plant J and Yamamoto Y 2002 Efficient source of single photons: a single quantum dot in a micropost microcavity *Phys. Rev. Lett.* **89** 233602
- [17] Claudon J, Bleuse J, Malik N S, Bazin M, Jaffrennou P, Gregersen N, Sauvan C, Lalanne P and Gerard J M 2010 A highly efficient single-photon source based on a quantum dot in a photonic nanowire *Nat. Photon.* **4** 174–7
- [18] Holmes M J, Choi K, Kako S, Arita M and Arakawa Y 2014 Room-temperature triggered single photon emission from a III-nitride site-controlled nanowire quantum dot *Nano Lett.* **14** 982–6
- [19] Jahn U, Lahnemann J, Pfuller C, Brandt O, Breuer S, Jenichen B, Ramsteiner M, Geelhaar L and Riechert H 2012 Luminescence of GaAs nanowires consisting of wurtzite and zinc-blende segments *Phys. Rev. B* **85** 45323
- [20] Graham A M, Corfdir P, Heiss M, Conesa-Boj S, Uccelli E, Fontcuberta I Morral A and Phillips R T 2013 Exciton localization mechanisms in wurtzite/zinc-blende GaAs nanowires *Phys. Rev. B* **87** 1–7
- [21] Rudolph D, Schweickert L, Morkötter S, Hanschke L, Hertenberger S, Bichler M, Koblmüller G, Abstreiter G and Finley J J 2013 Probing the trapping and thermal activation dynamics of excitons at single twin defects in GaAs–AlGaAs core–shell nanowires *New J. Phys.* **15** 113032
- [22] Vainorius N, Lehmann S, Jacobsson D, Samuelson L, Dick K A and Pistol M-E 2015 Confinement in thickness-controlled GaAs polytype nanodots *Nano Lett.* **15** 2652–6
- [23] Loitsch B, Winnerl J, Grimaldi G, Wierzbowski J, Rudolph D, Morkötter S, Döblinger M, Abstreiter G, Koblmüller G and Finley J J 2015 Crystal phase quantum dots in the ultrathin core of GaAs–AlGaAs core–shell nanowires *Nano Lett.* **15** 7544–51
- [24] Loitsch B et al 2015 Tunable quantum confinement in ultrathin, optically active semiconductor nanowires via reverse-reaction growth *Adv. Mater.* **27** 2195–202
- [25] Christen J, Bertram F, Schmidt G, Veit P, Petzold S, Ravash R, Dadgar A and Krost A 2012 Cathodoluminescence directly performed in a transmission electron microscope: nanoscale correlation of structural and optical properties *Microsci. Microanal.* **18** 1834–5
- [26] Schmidt G, Müller M, Veit P, Bertram F, Christen J, Glauser M, Carlin J-F, Cosendey G, Butté R and Grandjean N 2014 Nano-scale luminescence characterization of individual InGaN/GaN quantum wells stacked in a microcavity using scanning transmission electron microscope cathodoluminescence *Appl. Phys. Lett.* **105** 032101
- [27] Urban A, Müller M, Karbaum C, Schmidt G, Veit P, Malindretos J, Bertram F, Christen J and Rizzi A 2015 Optical emission of individual GaN nanocolumns analyzed with high spatial resolution *Nano Lett.* **15** 5105–9
- [28] Schmidt G et al 2015 Direct evidence of single quantum dot emission from GaN islands formed at threading dislocations using nanoscale cathodoluminescence: a source of single photons in the ultraviolet *Appl. Phys. Lett.* **106** 252101
- [29] Petroff P M 1987 Interface structure and optical properties of quantum wells and quantum boxes *J. Vac. Sci. Technol. B* **5** 1204
- [30] Mårtensson T, Svensson C P T, Wacaser B A, Larsson M W, Seifert W, Deppert K, Gustafsson A, Wallenberg L R and Samuelson L 2004 Epitaxial III–V nanowires on silicon *Nano Lett.* **4** 1987–90
- [31] Roest A L, Verheijen M A, Wunnicke O, Serafin S, Wondergem H and Bakkers E P A M 2006 Position-controlled epitaxial III–V nanowires on silicon *Nanotechnology* **17** S271–5

- [32] Plissard S, Dick K A, Larrieu G, Godey S, Addad A, Wallart X and Caroff P 2010 Gold-free growth of GaAs nanowires on silicon: arrays and polytypism *Nanotechnology* **21** 385602
- [33] Munshi A M et al 2014 Position-controlled uniform GaAs nanowires on silicon using nanoimprint lithography *Nano Lett.* **14** 960–6
- [34] Rudolph D, Schweickert L, Morkötter S, Loitsch B, Hertenberger S, Becker J, Bichler M, Abstreiter G, Finley J J and Koblmüller G 2014 Effect of interwire separation on growth kinetics and properties of site-selective GaAs nanowires *Appl. Phys. Lett.* **105** 033111
- [35] Rudolph D et al 2013 Spontaneous alloy composition ordering in GaAs-AlGaAs core-shell nanowires *Nano Lett.* **13** 1522–7
- [36] Fischer F, Grayson M, Schubert E, Schuh D, Bichler M and Abstreiter G 2004 New anisotropic behavior of quantum Hall resistance in GaAs heterostructures at mK temperatures and fractional filling factors *Phys. E Low-dimens. Syst. Nanostruct.* **22** 108–10
- [37] Williams D B and Carter C B 2009 *Transmission Electron Microscopy—A Textbook for Materials Science* (New York: Springer)
- [38] Rudolph D, Hertenberger S, Bolte S, Paosangthong W, Spirkoska D, Doblinger M, Bichler M, Finley J J, Abstreiter G and Koblmüller G 2011 Direct observation of a noncatalytic growth regime for GaAs nanowires *Nano Lett.* **11** 3848–54
- [39] Gustafsson A, Bolinsson J, Sköld N and Samuelson L 2010 Determination of diffusion lengths in nanowires using cathodoluminescence *Appl. Phys. Lett.* **97** 072114
- [40] Robinson H D and Goldberg B B 2000 Light-induced spectral diffusion in single self-assembled quantum dots *Phys. Rev. B* **61** R5086–9
- [41] Lambkin J D, Dunstan D J, Homewood K P, Howard L K and Emeny M T 1990 Thermal quenching of the photoluminescence of InGaAs/GaAs and InGaAs/AlGaAs strained-layer quantum wells *Appl. Phys. Lett.* **57** 1986
- [42] Xu Z Y, Lu Z D, Yang X P, Yuan Z L, Zheng B Z, Xu J Z, Ge W K, Wang Y, Wang J and Chang L L 1996 Carrier relaxation and thermal activation of localized excitons in self-organized InAs multilayers grown on GaAs substrates *Phys. Rev. B* **54** 11528–31
- [43] Williams F E and Eyring H 1947 The mechanism of the luminescence of solids *J. Chem. Phys.* **15** 289
- [44] Masumoto Y and Takagahara T 2013 *Semiconductor Quantum Dots: Physics, Spectroscopy and Applications* (Berlin: Springer)
- [45] Sell D D 1972 Resolved free-exciton transitions in the optical-absorption spectrum of GaAs *Phys. Rev. B* **6** 3750–3
- [46] Borri P, Langbein W, Hvam J M and Martelli F 1999 Well-width dependence of exciton-phonon scattering in $\text{In}_x\text{Ga}_{1-x}\text{As}/\text{GaAs}$ single quantum wells *Phys. Rev. B* **59** 2215–22
- [47] Gammon D, Snow E S, Shanabrook B V, Katzer D S and Park D 1996 Homogeneous linewidths in the optical spectrum of a single gallium arsenide quantum dot *Science* **273** 87–90
- [48] Besombes L, Kheng K, Marsal L and Mariette H 2001 Acoustic phonon broadening mechanism in single quantum dot emission *Phys. Rev. B* **63** 155307
- [49] Adachi S 1985 GaAs, AlAs, and $\text{Al}_x\text{Ga}_{1-x}\text{As}$ material parameters for use in research and device applications *J. Appl. Phys.* **58** R1
- [50] Gopal A V, Kumar R, Vengurlekar A S, Bosacchi A, Franchi S and Pfeiffer L N 2000 Photoluminescence study of exciton-optical phonon scattering in bulk GaAs and GaAs quantum wells *J. Appl. Phys.* **87** 1858